AD-A186 578 ADSORPTION OF PYRIDINE AT THE AU(100)-SOLUTION INTERFACE(U) WATERLOO UNIV (ONTARIO) DEPT OF CHEMISTRY L STOLBERG ET AL. 25 SEP 87 N00014-87-G-0110 1/1

UNCLASSIFIED F/G 7/4 NL

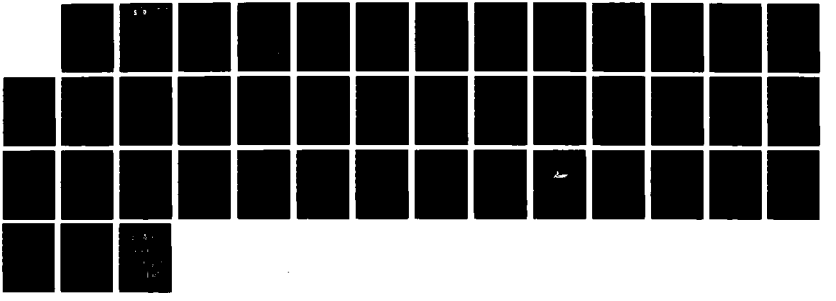

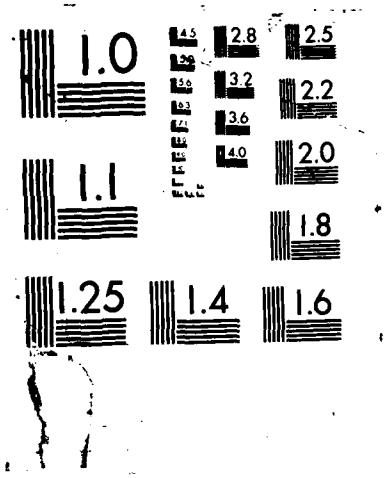
1.0
1.1
1.25
1.4
1.6
1.8
2.0
2.2
2.5
2.8
3.2
3.6
4.0

UNCLASSIFIED

(12)

AD-A186 578

REPORT DOCUMENTATION PAGE

DTIC FILE COPY

DTIC ELECTE OCT 19 1987 S D

Unclassified	1b. RESTRICTIVE MARKINGS
2a. SECURITY CLASSIFICATION AUTHORITY Unclassified	3. DISTRIBUTION / AVAILABILITY OF REPORT Public Release/Unlimited
2b. DECLASSIFICATION / DOWNGRADING SCHEDULE	
4. PERFORMING ORGANIZATION REPORT NUMBER(S) ONR Technical Report #1	5. MONITORING ORGANIZATION REPORT NUMBER(S)
6a. NAME OF PERFORMING ORGANIZATION D.E. Irish University of Waterloo	6b. OFFICE SYMBOL (If applicable)
7a. NAME OF MONITORING ORGANIZATION Office of Naval Research	
6c. ADDRESS (City, State, and ZIP Code) Department of Chemistry Waterloo, Ontario, Canada N2L 3G1	7b. ADDRESS (City, State, and ZIP Code) The Ohio State University, Research Center 1314 Kinnear Road Room 318 Columbus, Ohio 43212-1194 USA
8a. NAME OF FUNDING / SPONSORING ORGANIZATION Office of Naval Research	8b. OFFICE SYMBOL (If applicable)
9. PROCUREMENT INSTRUMENT IDENTIFICATION NUMBER N00014-87-G-0118	
8c. ADDRESS (City, State, and ZIP Code) Chemistry Division 800 N Quincy Street Arlington, VA 22217-5000 USA	10. SOURCE OF FUNDING NUMBERS PROGRAM ELEMENT NO. / PROJECT NO. / TASK NO / WORK UNIT ACCESSION NO

6 x 10 to the -10th mol/sq. cm

11. TITLE (Include Security Classification)

Adsorption of Pyridine at the Au(100) - Solution Interface

12. PERSONAL AUTHOR(S)
L. Stolberg, J. Lipkowski, D.E. Irish

13a. TYPE OF REPORT	13b. TIME COVERED	14. DATE OF REPORT (Year, Month, Day)	15. PAGE COUNT
Technical	FROM 1/87 TO 6/87	1987/9/25	39

16. SUPPLEMENTARY NOTATION
Presented in part at the 171st Meeting of the Electrochemical Society, Philadelphia, Penn. May 10-15, 1987 Abstract #438.

17. COSATI CODES		
FIELD	GROUP	SUB-GROUP

18. SUBJECT TERMS (Continue on reverse if necessary and identify by block number)
Chronocoulometry, Pyridine orientation and coverage, Free Energy of Adsorption, Au(100) Surface, Gold

19. ABSTRACT (Continue on reverse if necessary and identify by block number)

Chronocoulometry has been used in order to quantitatively characterize the energetics of pyridine adsorption onto a gold(100) single crystal electrode surface. Over the potential region investigated (-0.8 to +0.6 V), three orientations of the pyridine molecules on the gold surface have been observed. The pyridine orientation is strongly influenced by the electrode potential. At a positively charged surface, the pyridine assumes a verticle orientation with the nitrogen atom facing the gold surface. A limiting surface concentration corresponding to 6×10^{-10} mol cm^{-2} was determined for the vertical orientation. At a negatively charged surface and at low surface concentrations ($\Gamma < 1 \times 10^{-10}$ mol cm^{-2}) the pyridine molecules adsorb flat with the aromatic rings oriented parallel to the surface. At intermediate surface concentrations (3×10^{-10} mol cm$^{-2} > \Gamma > 1 \times 10^{-10}$ mol cm^{-2}) and for potentials close to zero charge, a third orientation presumably intermediate betweenthe flat and the vertical orientations was observed. Reorientation from the intermediate to the vertical orientation takes the form of a phase transition. The potential of the phase transition approximately coincides with the potential of zero charge. The free energies of adsorption, electrosorption valencies, potentials and charges of the maximum adsorption were determined for the flat and the vertical orientation of pyridine. Adsorption of pyridine on the Au(100) surface is compared with the adsorption at polycrystalline Au and mercury electrodes.

20. DISTRIBUTION / AVAILABILITY OF ABSTRACT	21. ABSTRACT SECURITY CLASSIFICATION
☒ UNCLASSIFIED/UNLIMITED ☐ SAME AS RPT. ☐ OTIC USERS	Unclassified
22a. NAME OF RESPONSIBLE INDIVIDUAL Donald E. Irish	22b. TELEPHONE (Include Area Code) (519)885-1211 Ext 2500
	22c. OFFICE SYMBOL

DD FORM 1473, 84 MAR 83 APR edition may be used until exhausted. All other editions are obsolete.

SECURITY CLASSIFICATION OF THIS PAGE

Unclassified

OFFICE OF NAVAL RESEARCH

Contract N00014-87-G-0118

R & T Code 4133016

Technical Report No. 1

Adsorption of Pyridine at the Au(100)-Solution Interface

by

L. Stolberg, J. Lipkowski, and D.E. Irish

Prepared for Publication

in

J. Electroanal. Chem.

University of Waterloo

Department of Chemistry

Waterloo, Ontario

Canada, N2L 3G1

September 25, 1987

corrected

ADSORPTION OF PYRIDINE AT THE Au(100)-SOLUTION INTERFACE

L. Stolberg and J. Lipkowski

Guelph-Waterloo Centre for Graduate Work in Chemistry
Guelph Campus
Department of Chemistry and Biochemistry
University of Guelph
Guelph, Ontario N1G 2W1
Canada

D.E. Irish

Guelph-Waterloo Centre for Graduate Work in Chemistry
Waterloo Campus
Department of Chemistry, University of Waterloo
Waterloo, Ontario N2L 3G1
Canada

ABSTRACT

Chronocoulometry has been used in order to quantitatively characterize the energetics of pyridine adsorption onto a gold(100) single crystal electrode surface. Over the potential region investigated (-0.8 to +0.6 V), three orientations of the pyridine molecules on the gold surface have been observed. The pyridine orientation is strongly influenced by the electrode potential. At a positively charged surface, the pyridine assumes a vertical orientation with the nitrogen atom facing the gold surface. A limiting surface concentration corresponding to 6×10^{-10} mol cm^{-2} was determined for the vertical orientation. At a negatively charged surface and at low surface concentrations ($\Gamma < 1 \times 10^{-10}$ mol cm^{-2}) the pyridine molecules adsorb flat with the aromatic rings oriented parallel to the surface. At intermediate surface concentrations (3×10^{-10} mol $cm^{-2} > \Gamma > 1 \times 10^{-10}$ mol cm^{-2}) and for potentials close to zero charge, a third orientation presumably intermediate between the flat and the vertical orientations was observed. Reorientation from the intermediate to the vertical orientation takes the form of a phase transition. The potential of the phase transition approximately coincides with the potential of zero charge. The free energies of adsorption, electrosorption valencies, potentials and charges of the maximum adsorption were determined for the flat and the vertical orientation of pyridine. Adsorption of pyridine on the Au(100) surface is compared with the adsorption at polycrystalline Au and mercury electrodes.

Introduction

This work is part of a project which is devoted to studying the influence of crystallographic orientation of gold electrodes on the adsorption of neutral organic molecules from aqueous electrolyte solutions. Using combined electrochemical and spectroscopic techniques we are trying to determine how the orientation of the adsorbed molecule and energetics of its adsorption are governed by the geometry and density of coordination centres present at the electrode surface.

Pyridine is an ideal molecule for combined electrochemical and spectroscopic investigations. Pyridine is SERS active on gold [1] and its principle vibrational bands do not overlap with those of water so it may be probed by IR spectroscopy as well. Finally, as we have shown recently, the energetics of its adsorption on gold may be determined using chronocoulometry [2]. Previously, Hamelin [3] investigated pyridine adsorption on gold single crystal electrode surfaces using differential capacity. These works have provided qualitative information on pyridine adsorption and have shown that there is a strong influence of the surface morphology on the adsorption process.

In this communication, the energetics of pyridine adsorption onto the gold(100) surface will be described. Quantitative data such as adsorption isotherms, Gibbs energies of adsorption and electrosorption valencies will be given. Spectroscopic data will be presented in a future communication.

Experimental

Solutions

All solutions were prepared from Milli-Q water (Waters). The supporting electrolyte was 0.1 M $KClO_4$. $KClO_4$ (ACS Certified from Fisher) was purified by calcinating at 300° C, recrystallizing twice from

Milli-Q water, and then drying. Pyridine (ACS Certified from Fisher) was used without further purification. Pyridine solutions ranging in concentration from 10^{-5} M to 10^{-2} M were investigated. They were prepared from a 0.1M pyridine stock solution. All the solutions were degassed with argon for at least 1h before each experiment. During the experiment argon was passed over the top of the solution. All experiments were carried out at 25 ± 1°C.

Electrodes

The working electrode was a gold(100) single crystal rod (99.99% Johnson Matthey) prepared according to the Bridgeman technique [4]. The single crystal was oriented using the back Laue diffraction technique. The gold rod was then polished to a smooth finish with succeedingly finer grades of alumina ending with the 0.05 μm grade. Once polished, the electrode was annealed for approximately 3 h at a temperature of about 700° C. The counter electrode consisted of a gold coil. An external saturated calomel electrode (SCE) was used as the reference electrode. All potentials reported are relative to the SCE. Before each experiment the gold working electrode was flamed three times and then quenched after flaming with Milli-Q water [5]. In all electrochemical experiments the hanging electrolyte technique was used [6].

Kolb et al., [7, 8] (also see comment by Hamelin [9]) have shown recently that the Au(100) surface, when prepared by flaming and quenching, has a reconstructed (5 x 20) surface. The reconstructed surface is stable at the metal solution interface provided the electrode is not exposed to polarizations higher then +0.55 V. When the anodic limit of the applied potential exceeds +0.60 V the reconstruction is lifted and the (1 x 1) structure appears. The (5 x 20) → (1 x 1) transition is irreversible in the sense that the electrode has to be flamed and quenched once again to restore

the (5 x 20) structure. In our work a potential sweep up to +1.1 V, as the anodic limit, was applied just after contact between the electrode and the electrolyte was made. In view of Kolb's results, all our experiments were performed with the surface having the (1 x 1) structure. Instrumentation and the time sequence of the different steps involved in the data acquisition and processing have been described in previous papers [2, 10].

Results and Discussion

(i) Experimental Strategy

The experimental strategy used in this work involved the following steps: a) characterization of the surface by recording cyclic voltammograms and differential capacity curves, b) determination of the electrode charge density, σ_M, from chronocoulometric experiments, c) back integration of the σ_M with respect to potential curves to calculate the film pressure π, d) calculation of the relative Gibbs excesses, e) determination of the Gibbs energy of adsorption. These steps will be described under separate paragraphs.

(ii) Cyclic Voltammetry

Cyclic voltammograms were recorded in order to: a) ensure qualitatively that the electrode surface was free from contamination, b) determine the potential range in which the electrode is behaving as an ideally polarisable electrode, and c) detect the presence of oxygen in the solution and creeping of the solution on the walls of the electrode. The creeping effect, and the presence of oxygen, result in a characteristic distortion of the double layer region of the cyclic voltammogram.

Shown in Figure 1 are two cyclic voltammograms which have been obtained for the gold(100) single crystal electrode in both the absence and presence of pyridine, Figures 1a and b respectively. The cyclic voltammogram presented for the supporting electrolyte alone agrees well with those which have previously been reported [11]. It was always found that precisely repeatable cyclic voltammograms could be obtained after about four cycles. This strongly suggests that the solutions being investigated were always of high purity and free from oxygen. No distortion due to the creeping effect was observed.

There are a number of subtle differences between the cyclic voltammograms obtained for gold(100) in the absence and presence of pyridine. As Figure 1b shows, pyridine adsorption/desorption peaks are apparent at negative potentials. At electrode potentials greater than +0.6 V oxidation of the gold surface takes place. Comparing Figures 1a and b, it is evident that pyridine is having a significant influence on the oxidation of gold. The cyclic voltammogram which was obtained for the supporting electrolyte alone shows the presence of at least four peaks in the oxidation region. In contrast the cyclic voltammogram obtained in the presence of pyridine shows only one peak.

Integration of the anodic branches of the cyclic voltammograms obtained in the absence and presence of pyridine for potentials greater than +0.6 V showed that the charge is 1.36 times greater when pyridine is present in the solution. This suggests that the pyridine molecules are being partially oxidized at the gold(100) electrode surface. Integration of the cathodic branches of the two cyclic voltammograms showed that the charges were equal This indicates that the same amount of oxide was deposited in the anodic half of the cycle for the two cases and that the pyridine oxidation is irreversible.

In conclusion, Figures 1a and b show that the double layer region of the gold electrode extends from -0.8 to +0.6 V. In this potential region the gold(100) electrode is behaving as an ideally polarisable electrode.

(iii) Differential Capacity

Differential capacity curves have been recorded in order to determine the potential and concentration range for which pyridine is adsorbed onto the gold surface. In addition, it has been used to determine the potential of zero charge (pzc) from the position of the diffuse layer minimum.

Shown in Figure 2a are two differential capacity curves which have been obtained for the Au(100) single crystal electrode in the presence of 10^{-2} M and 10^{-1} M $KClO_4$. The capacity curves (Figures 2a and b) have been recorded when a potential sweep of 5 mVs^{-1} in the anodic direction was applied. On the reverse sweep (which is not shown in Figure 2) considerable hysteresis was found. The hysteresis was observed irrespective of whether pyridine was absent or present in the electrolyte solution. The degree of hysteresis depended strongly on the anodic limit of the forward sweep. Similar hysteresis was observed earlier by Hamelin [11] and Kolb et al. [7, 8]. The capacity curve, which was obtained in the presence of 10^{-2} M $KClO_4$, displays a, diffuse layer minimum at approximately +0.14 V which corresponds to the potential of zero charge. This value is in excellent agreement with the data reported by Hamelin and Lecoeur [12, 13]. Qualitatively, our capacity curve (recorded in 10^{-2} M $KClO_4$) is in reasonable agreement with that which has been published by Kolb et al. [7, 8]. However, the value of the pzc (+0.06 V) reported in their paper is lower than our result. Incidentally, Lecoeur et al. [13] measured the pzc for a number of crystallographic orientations vicinal to the (100) plane. They showed that the value of the pzc strongly depends on the density of surface imperfections such as monoatomic steps. The pzc shifts in the negative direction when the density of imperfections increases. Therefore, the lower value of the pzc reported in reference [7, 8] may indicate that the surface used in these investigations contained a large density of imperfections.

Shown in Figure 2b are two capacity curves which have been obtained for Au(100) in the presence of 10^{-4} M and 6.2×10^{-3} M pyridine. Differential capacity curves for the lowest pyridine concentrations studied have not been presented here because they were strongly frequency dependent due to mass transport limitations. The differential capacity curves display two peaks.

The peak with a shoulder, which appears at negative electrode potentials, is characteristic of the pyridine adsorption/desorption process. This peak shifts towards more negative potentials and its magnitude increases with increasing pyridine concentration. Furthermore, at pyridine concentrations greater than 10^{-4} M a capacity peak at anodic electrode potentials appears. For the pyridine concentration range studied, it is found that the height of this peak is independent of the bulk pyridine concentration. However, the position of this peak is found to shift toward more negative potentials with increasing pyridine concentrations. This peak may correspond to several different processes. The possibilities will be discussed shortly.

Overall, the differential capacity curves, which have been obtained in the presence of pyridine, have shown that, at E ≃ -0.8 V and for pyridine concentrations below 10^{-2} M, the capacity curves merge with the capacity curve for the supporting electrolyte (10^{-1}M $KClO_4$). This indicates that at E = -0.8 V and for pyridine concentrations below 10^{-2} M, pyridine is totally desorbed from the electrode surface. At higher pyridine concentrations, pyridine desorption overlaps with hydrogen evolution. At E ≃ +0.6 V, the oxidation of gold begins. At pyridine concentrations below 10^{-5} M the rate of mass transport to the surface is so small that one has to wait a few minutes for the adsorption equilibrium to be established. Therefore, the pyridine adsorption studies were restricted to the potential range -0.8 V to +0.6 V and to a concentration range 10^{-5} to 10^{-2} M pyridine.

(iv) Step Experiments

Step experiments involved holding the electrode at an initial potential E_i, where pyridine adsorption takes place, for 2 min. This time was long enough for the adsorption equilibrium to be established. Then the potential was stepped to E_f = -0.8 V and the double layer charging currents were

recorded.

Shown in Figure 3a are current transients which have been obtained for the gold(100) electrode in the presence of 6.2×10^{-3} M pyridine at various electrode potentials. The current and time axis are in the plane of the figure while the potential axis is normal to this plane. The time window in which the transients were recorded was the same for both the supporting electrolyte and for solutions containing pyridine. In fact, the rate determining step in the charging of the double layer is the same in both cases, and the kinetics is limited by the time constant of the cell, RC. From Figure 3a one can see that the current decreases monotonically with time for potentials more negative then -0.2 V, while above this value a hump appears in the transients. From the differential capacity curves (Figure 2b), we realize that the appearance of this hump coincides with an increase in the capacity. This hump can be explained in terms of the dependence of the time constant (RC) of the cell on time [10].

The current-time transients displayed in Figure 3a were recorded over a 10 ms time window. In addition, current-time transients were also recorded over a 100 ms time window and were digitally integrated to yield the charge-time transients. Shown in Figure 3b are the $\Delta\sigma_M$-t curves which have been obtained for the 6.2×10^{-3} M pyridine solution. Note, that for the sake of display, the direction of the time axis has been reversed in Fig. 3b. Here, $\Delta\sigma_M$ is the relative charge density which is given by the following equation:

$$\Delta\sigma_M(E_i) = \sigma_M(E_i) - \sigma_M(E = -0.8\ V) \qquad (1)$$

where σ_M is the absolute charge density. A three dimensional presentation of the data is once again shown. In this case the charge and time axis are in the plane of the figure and the potential axis is normal to this plane.

For both the supporting electrolyte and for solutions containing pyridine, the $\Delta\sigma_M$ - t curves display a well defined plateau where the charge is essentially independent of time over the whole potential range investigated. The section of the chronocoulometric curve corresponding to the plateau region was extrapolated by linear regression to t = 0. This procedure ensured that the data were corrected for instrumental offsets and/or parasitic faradaic currents. The extrapolated charge was equal to the charge difference between the equilibrium charge densities at the potential E_i and E = -0.8 V.

(v) Charge-Potential Plots

The relative charge density data allowed the absolute charge density, σ_M, for the base solution and for the various pyridine concentrations to be calculated. From the potential of zero charge, which has been independently measured, and from equation (1), σ_M (-0.8 V) was determined:

$$\Delta\sigma_M(pzc) = \sigma_M(pzc) - \sigma_M(-0.8\ V) = -\sigma_M(-0.8\ V) \qquad (2)$$

From σ_M(-0.8 V) and equation (1), values of $\sigma_M(E_i)$ were calculated over the whole potential range investigated.

Presented in Figure 4 are the σ_M - E curves which have been obtained for the gold (100) electrode in both the absence and presence of pyridine. At the most negative electrode potentials the σ_M - E curves for the various pyridine concentrations are seen to merge with the curve for the supporting electrolyte. This shows that, at these potentials, the pyridine molecules are totally desorbed from the gold surface. There is no evidence for pyridine desorption at the far anodic potentials.

The most striking feature of Figure 4 is an abrupt change in the value of the charge density such that the charge density curve has the appearance of a step function. The height of this step spans approximately 20 $\mu C\ cm^{-2}$

and the charge density changes sign (zero charge density is located approximately in the middle of the step). This behaviour is typical of a phase transition. The potential at which this phase transition occurs is very close to pzc in the given solution and depends on the bulk pyridine concentration. It was found to shift towards more negative potentials with increasing bulk pyridine concentrations.

Following the phase transition, the absolute charge densities, which are now positive, are essentially concentration independent indicating that the surface concentration of pyridine reached a maximum (saturation) value Γ_{max}. Initially, in this section of the curve, the charge density, as expected, depends almost linearly on the electrode potential. Extrapolation of this segment to $\sigma_M = 0$ allowed us to determine the shift of the potential of zero charge, E_N given by the following equation [14, 15]:

$$E_N = \frac{4\pi\bar{\mu}}{\epsilon}\Gamma_{max} \qquad (3)$$

where $$\bar{\mu} = \mu^{org} - n\mu^{w} \qquad (4)$$

μ^i is the component of the dipole moment perpendicular to the gold (100) surface, i stands for the organic and water molecules respectively, n is the number of water dipoles replaced at the surface by one pyridine molecule and ϵ is the dielectric constant of the inner layer. The pzc shifts in the negative direction and the value of E_N was found to be -0.795 V. The negative value found for E_N indicates that $\bar{\mu}$ is negative. The effective dipole moment $\bar{\mu}$ could be negative if either (a) $|n\mu^w| > |\mu^{org}|$ and $\mu^w > 0$ or (b) $|\mu^{org}| > |n\mu^w|$ and $\mu^{org} < 0$. The first possibility may be rejected because a positive value of μ^w would indicate that the water molecules are oriented with the hydrogen atoms facing the metal side of the interface. On the basis of independent arguments [16], it is known that Au(100) is

slightly hydrophilic and the gold-water interactions orient the water molecules preferentially with the oxygen atom facing the metal side of the interface. The second possibility (b) indicated that the effective dipole moment of the organic molecule must be negative. This shows that the pyridine molecule is oriented with nitrogen facing the metal and the hydrocarbon part facing the solution side of the interface.

At potentials more positive than +0.35 V the σ_M - E curves start to diverge. This coincides with the appearance of the anodic peak on the capacity curves. The origin of these behaviours will be discussed shortly.

(vi) Film and Surface Pressure Curves

The relative interfacial tension, γ, was obtained by integrating σ_M with respect to E according to the equation:

$$\gamma(E_i) = \int_{-0.8V}^{E_i} \sigma_M dE + \gamma(-0.8\ V) \qquad (5)$$

The integration constant $\gamma(-0.8\ V)$ is not known but its value is independent of the pyridine concentration (since we have no adsorption at -0.8 V). Next, the film pressure, π, was determined from the relative interfacial tension using the following expression:

$$\pi(E_i) = \gamma_{\theta=0} - \gamma_\theta = \int_{-0.8V}^{E_i} \sigma_{M,\theta=0} dE - \int_{-0.8V}^{E_i} \sigma_{M,\theta} dE \qquad (6)$$

Shown in Figure 5a are plots of π versus E for the various pyridine concentrations investigated. Independently, at constant charge, the surface pressure ϕ was calculated from the Parson's function ξ(i.e., $\xi = \gamma + \sigma_M E$ and $\phi = \xi_{\theta=0} - \xi_\theta$) [17]. Shown in Figure 5b are plots of ϕ versus σ_M for the various pyridine concentrations studied. Qualitatively, the results in Figure 5a and b are very similar, keeping in mind that a charge density of 20 $\mu C\ cm^{-2}$ corresponds to an electrode potential approximately equal to

+0.15 SCE V .

For the lowest pyridine concentrations, the film and surface pressure curves display two maxima. One of these is shallow and located in the range E = +0.05 V to -0.05 V and σ_M = -4 to -8 μC cm^{-2}. Because of the expanded ϕ axis, this is more visible on the surface pressure plot than it is on the film pressure plot. The second maximum can be seen at E = +0.4 V and σ_M = +34 μC cm^{-2}. This is more apparent on the film pressure plot because of the wider range of E covered. This suggests that, in the potential (charge) range investigated, the pyridine molecules assume two different orientations on the gold surface. Clearly the shape of the π or ϕ curves, shown in Figure 5a and b, can be understood as arising from the superimposition of two bell shaped curves corresponding to each of the two orientations.

At the positively charged surface the film or surface pressures reach fairly large values (>100 mN m^{-1}) at moderate pyridine concentrations. This indicates that the zero coverage Gibbs energy of adsorption and/or the energy of attractive latteral interactions for this orientation are large.

(vii) Adsorption Isotherms

By graphical differentiation of the film pressure versus logarithm of the bulk pyridine concentration curves, the relative Gibbs surface excesses were calculated[2]. Presented in Figure 6 are plots of the relative Gibbs surface excess as a function of the electrode potential for the various pyridine concentrations investigated. Shown in Figure 7 are the adsorption isotherms (Γ versus lnc) which have been obtained at constant electrode potential. The isotherms presented here span the potential region -0.5 to +0.1V. For electrode potentials more negative then -0.2 V only segments of the isotherms were determined due to the limited range of pyridine concentrations investigated. The phase transition already observed on the

charge-potential curves appears in Figures 6 and 7 as an abrupt change in the relative Gibbs surface excess. As Figure 6 and 7 show, a plateau at a surface concentration of 6×10^{-10} mol cm^{-2} is present. This limiting value of the surface concentration (i.e., saturation coverage), is consistent with the pyridine molecules present on the surface in the vertical orientation [18]. From considering the shift in the pzc the same conclusion was reached earlier.

It is necessary to point out that Γ values in the region of the phase transition are less precise than the Γ values determined before or after the phase transition. This added error arises from the large curvature of the π versus lnc plots which reduces the precision of the graphical differentiation. For this reason the curves in Figures 6 and 7 have been represented by a dotted line once a surface concentration of 3.0×10^{-10} mol cm^{-2} is reached. This approach has been used to emphasize the large uncertainty of Γ in this region. At potentials more positive then +0.4 V the limiting surface concentration rises again (Figure 6). This increase coincides with the position of the anodic peak on the differential capacity curves. The increase of Γ as well as the appearance of the capacity peak may be caused by a number of processes such as further reorientation of the pyridine molecules, multilayer adsorption, or incipient oxidation of the gold surface. At present, we are unable to point out which of them is the most likely phenomenon which is occurring. Therefore, further analysis of the data will be limited to potentials negative of E = +0.4 V.

(viii) Potential Drop Across The Inner Layer

In order to gain further insight into the structure of the inner layer it is worthwhile to consider the dependence of the potential drop across the inner layer on the relative Gibbs surface excess.

According to a simple electrostatic model, the potential difference across the inner layer region of the double layer is given by [14, 15]

$$\Delta_2^M\phi = (4\pi/\epsilon)(\sigma_M x_2 + \Gamma\bar{\mu}) \tag{7}$$

where ϵ is the dielectric constant of the inner layer, x_2 is the thickness of the inner layer and $\bar{\mu}$ is the effective dipole moment as defined in equation (4). The potential drop across the inner layer can be taken approximately as:

$$\Delta_2^M\phi = E - E_{pzc} - \phi_2 \tag{8}$$

where E_{pzc} is the potential of zero charge in the absence of surfactant and ϕ_2 is the potential drop across the diffuse layer which can be calculated from the experimental values of σ_M using the classical Gouy-Chapman theory.

Shown in Figure 8 are plots of $\Delta_2^M\phi$ versus Γ for the various negative charge densities indicated. These plots cover the Γ range which is below the phase transition. Surface concentration values, which are greater than approximately 3×10^{-10} mol cm^{-2}, are not shown in the figure because of large uncertainties in the value of Γ. As the figure shows, the plots corresponding to $\sigma_M > -14$ μC cm^{-2} are clearly nonlinear which indicates that a reorientation of the pyridine molecules takes place [19]. The shape can be approximately represented by two straight line segments as in the case of pyridine adsorption onto mercury [20]. The two straight line segments correspond to the adsorption of pyridine in two different orientations. This is clearly visible at the zero charge density because the slopes of the two segments are of opposite signs.

According to equation (7) the potential drop across the inner layer for $\sigma_M = 0$ is given by:

$$\Delta_2^M\phi = (4\pi/\epsilon)\Gamma\bar{\mu} \tag{9}$$

Since ϵ and Γ are always positive, a change in the sign of the slope of the $\Delta_2^M\phi$ versus Γ plot must mean that the sign of the effective dipole moment perpendicular to the surface has changed. This can be understood in terms of two different orientations with different dipole moments perpendicular to the surface. One orientation is seen for $\Gamma < 1 \times 10^{-10}$ mol cm^{-2} while a second orientation is present for $\Gamma > 1 \times 10^{-10}$ mol cm^{-2}. This is significant since it shows that a reorientation of the pyridine molecules takes place before the onset of the phase transition.

(ix) Free Energy of Adsorption

The free energy of adsorption is usually determined from a fit of experimental data to an equation of an adsorption isotherm [21]. An isotherm which takes into account reorientation of the adsorbed molecules with coverage has to have the form of a multiparameter expression. A fit of such an expression to experimental data must necessarily be ambiguous. However, in the limit of zero coverage the adsorption of pyridine must be described by the Henry's law isotherm. The film pressure should then linearly depend on the bulk pyridine concentration as described by the following equation:

$$\pi = RT\Gamma_{max}\beta X_b \tag{10}$$

where π is the film pressure, X_b the mole fraction of pyridine in the solution and Γ_{max} is the limiting surface concentration. The adsorption coefficient β is related to the Gibbs energy of adsorption through the equation:

$$\Delta\bar{G}^\circ = -RT\ln\beta \tag{11}$$

The Gibbs energy of adsorption corresponds to the standard state being unit mole fraction of pyridine in the bulk of the solution and unit coverage at the surface (unsymmetrical choice of the standard state [22]). The

coefficient β can be determined from the initial slopes of the film pressure versus bulk pyridine concentration plots which in view of equation 10 should be equal to:

$$\beta = \left(\frac{\partial \pi}{\partial X_b}\right)_{X_b \to 0} / RT\Gamma_{max} \qquad (12)$$

This procedure was used to determine the adsorption coefficients for the potential range -0.45 V to +0.15 V. For reasons discussed later, Γ_{max} corresponding to 3×10^{-10} mol cm^{-2} was taken in these calculations. Finally, values of $\Delta\bar{G}°$ were determined with the help of equation 11.

Shown in Figure 9 is a plot of $\Delta\bar{G}°$ versus E. One can see from this figure that $\Delta\bar{G}°$ depends on E in a parabolic way. The maximum value of $\Delta\bar{G}°$ is equal to -36 $kJmol^{-1}$ and the potential at which this value occurs is approximately +0.05 V.

The first derivative of $\Delta\bar{G}°$ versus E is equal to the electrosorption valency γ. Incidentally, the electrosorption valency may also be determined from the dependence of the charge density on the surface concentration of pyridine at constant electrode potential.

With the help of simple thermodynamic arguments, it is easy to show that [23]:

$$\gamma = \left(\frac{1}{F}\right)\left(\frac{\partial \mu_p}{\partial E}\right)_\Gamma = \left(\frac{1}{F}\right)\left(\frac{\partial \Delta\bar{G}°}{\partial E}\right)_\Gamma = -\left(\frac{1}{F}\right)\left(\frac{\partial \sigma_M}{\partial \Gamma}\right)_E \qquad (13)$$

The slopes of the σ_M versus Γ plots can then be compared to the first derivative of the $\Delta\bar{G}°$ versus E plots. This can be used to check the consistency of our results.

Shown in Figure 10 is a plot of σ_M versus Γ for the various electrode potentials investigated. Once again our analysis was restricted to small values of the surface concentration. As the figure shows, linear

relationships are observed for the whole potential and surface concentration range investigated. The slope of the straight lines, which gives the electrosorption valency, depends on the value of the electrode potential.

Shown in Figure 11 are two plots of γ versus E which have been obtained from the slope of the σ_M versus Γ plots and by differentiation of the $\Delta\bar{G}°$ versus E plot. As the figure shows, there is no quantitative agreement between the two sets of data. These differences indicate that the γ values are subject to errors due to: a) the large spread of the experimental points in Figure 10 and/or b) the approximate nature of the extrapolation procedure used to determine β, c) errors due to the graphical differentiation of the $\Delta\bar{G}°$ - E curve. However, the two sets of data vary with potential in a quasilinear way indicating a quasiquadratic dependence of the free energy of adsorption on the electrode potential. Moreover, the two plots intersect the zero line at +0.03 V and +0.05 V respectively giving similar values of the potential of maximum adsorption.

(x) Anion Effect

Differential capacity curves and electrode charge densities were determined for gold(100) in a solution containing 10^{-1} M NaF and 10^{-3} M pyridine in order to see if the anion is having any influence on pyridine adsorption.

Shown in Figure 12a is the differential capacity curve which has been obtained for Au(100) in the presence of 10^{-1} M NaF and 10^{-3} M pyridine; for comparison the data obtained for gold(100) in the presence of 10^{-1} M $KClO_4$ and 10^{-3} M pyridine are also shown. One can see that in the presence of fluoride there is an additional capacity peak at negative electrode potentials. At positive electrode potentials, the capacity peak observed in the presence of fluoride is much larger. Actually, the differential

capacity curve determined for pyridine adsorption from fluoride solution is very similar to the curve reported by Hamelin [3] for pyridine adsorption onto Au(100) from a sulphate electrolyte. This shows that the fluoride and sulphate ions are influencing pyridine adsorption in a similar manner.

Shown in Figure 12b are the absolute charge density-potential curves which have been obtained for gold(100) in the solutions described above. As the figure shows, the hump observed at negative electrode potentials is broader in the case of fluoride then it is in the case of perchlorate. The σ_M - E curve obtained for the fluoride solution shows that the phase transition is shifted approximately 0.05 V in the anodic direction. For anodic electrode potentials the charge is considerably larger when fluoride is present in the solution. However, the differences between pyridine adsorption from NaF and $KClO_4$ solutions are quantitative but not qualitative. The main features such as different adsorption at the positively and negatively charged surface and the presence of the phase transition are displayed in both electrolytes. The nature of the electrolyte influences mainly the stability range of the different structures of the film of adsorbed pyridine.

Summary and Conclusions

Our data have shown that there are three different orientations possible for the pyridine molecules on the gold(100) surface over the entire potential region investigated. Two of these orientations, which we will call A and B, exist prior to the phase transition and are found on a negatively charged surface. Orientation A is present for $\Gamma < 1 \times 10^{-10}$ mol cm^{-2} and for the most negative electrode potentials while orientation B is observed for 3×10^{-10} mol $cm^{-2} > \Gamma > 1 \times 10^{-10}$ mol cm^{-2} and for potentials close to the potential of zero charge. The third orientation, which we will

call C, is observed after the phase transition on a positively charged surface; it corresponds to $\Gamma \tilde{=} 6 \times 10^{-10}$ mol cm^{-2}. Orientation A and C are the major orientations while B is an intermediate orientation. The phase transition takes place between orientations B and C.

Presented in Table 1 are the important adsorption parameters which have been determined for pyridine adsorption onto the gold(100) electrode surface in orientations A and C. For comparison, data for pyridine adsorption onto a polycyrstalline gold electrode surface and onto a mercury electrode surface are also included.

Consider first orientation A. The shift in the potential of zero charge, E_N, is small and indicates that for this orientation the component of the dipole moment in the direction normal to the surface is small as well. The maximum value of $\Delta\bar{G}°$ found for orientation A is -36 kJ mol^{-1}. This value is similar to that observed for pyridine adsorption onto a polycrystalline gold electrode surface (-38 kJ mol^{-1}) [2] and is almost twice the value observed for pyridine adsorption onto mercury (-19 kJ mol^{-1}) [25]. This large absolute value for $\Delta\bar{G}°$ indicates that a strong specific interaction takes place between the pyridine molecules and the gold(100) electrode surface. These are strong arguments that in orientation A the pyridine molecules are adsorbed flat at the surface. Support for this conclusion comes from a UHV study carried out by Demuth et al. [24] on pyridine adsorption onto the silver(111) plane. They found that, for low coverages ($< 3 \times 10^{14}$ molecules/cm^2), the pyridine molecules assume the flat orientation with an angle of inclination corresponding to 3°. Strong coupling of the bonding π orbitals of the pyridine molecule to the unoccupied electronic states in the metal band structure was concluded in that case. It is likely that pyridine adsorption at gold has exactly this same character.

Based on these arguments, a value of Γ_{max} corresponding to 3×10^{-10} mol cm^{-2} was used in calculating $\Delta\bar{G}°$ from the Henry's law isotherm. This value of Γ_{max} was determined for the flat orientation of adsorbed pyridine molecules by Conway et al. [18]. For orientation C, E_N is large and negative. This indicates that the component of the effective dipole moment in the direction normal to the surface is large and that the negative pole of the dipole is directed toward the metal. Based on the experimental value for Γ_{max} (6×10^{-10} $molcm^{-2}$), and the above, we conclude that the pyridine molecules are present on the gold(100) surface in the vertical orientation with the nitrogen atom facing the gold surface. Further evidence for the vertical orientation comes from the existence of the phase transition. The presence of the phase transition indicates that strong lateral interactions take place between the adsorbed pyridine molecules. It is well known that aromatic heterocyclics strongly interact laterally when adsorbed in the vertical position. [26]

For pyridine adsorption from the gas phase onto a silver(111) surface Demuth et al., [24] observed that, for large coverages, the pyridine molecules assume the vertical orientation. Strong coupling of the non-bonding molecular orbitals on the nitrogen atoms to the empty electronic states in the metal was observed. They found also that the pyridine molecules are adsorbed at an angle of inclination of approximately 55° to the silver surface. At that angle, an overlap between occupied non-bonding orbitals on the nitrogen atoms and the empty antibonding π orbitals of a contiguous pyridine molecule takes place. This explains the presence of strong lateral interactions between adsorbed pyridine molecules. Once again this same molecular model may be adopted to describe the pyridine adsorption at the Au(100) surface at large coverages.

Table 1 shows that the magnitude of E_{max} and σ_{max} strongly depends on the molecule orientation and the nature of the substrate. Actually, the variation of the charge and the potential of the maximum adsorption reflects changes in the shift in potential of zero charge E_N. These quantities are relatd by the following equations derived from the model of two parallel capacitors [27]:

$$E_{max} - E_{pzc} = -E_N \, C_{\theta=1}/(C_o - C_{\theta=1}) \tag{14}$$

and

$$\sigma_{max} = -E_N \, C_{\theta=1} \, C_o/(C_o - C_{\theta=1}) \tag{15}$$

where C_o and $C_{\theta=1}$ denote the differential capacities of the double layer in the pure supporting electrolyte solution and at complete surface coverage with pyridine, respectively.

For orientation A, E_N is small and positive and in agreement with the above equations the absolute values of $E_{max} - E_{pzc}$ and σ_{max} are small and their sign is negative. For orientation C the absolute value of E_N is large and its sign is negative and as predicted by equations 14 and 15 the values of $E_{max} - E_{pzc}$ and σ_{max} are positive and large. For the vertical orientation of the pyridine molecules on mercury E_N is large and positive and as expected $E_{max} - E_{pzc}$ and σ_{max} are negative and their absolute values are large. This result indicates that, in agreement with Frumkin predictions [27, 28], the magnitude of E_{max} and σ_{max} is primarily determined by the magnitude and the orientation (negative or positive pole facing the metal) of the component of the permanent dipole moment of the adsorbed molecule in the direction normal to the surface. In other words on the polarity of the adsorbed molecule.

The potential range in which adsorption takes place is determined by the magnitude of the parameter b which in terms of the parallel capacitors model can be expressed by [27]:

$$b = (C_o - C_{\theta=1})/2RT\Gamma_{max} \qquad (16)$$

Unfortunately, we do not have precise data for $C_{\theta=1}$ to compare the experimental values of b determined for orientations A and C with the values calculated with the help of equation 16. However, it is generally expected that the term $(C_o - C_{\theta=1})$ is small for flat and large for the vertical orientation of the adsorbed molecule. In agreement with this predication, the value of b determined for orientation A is much smaller than the value found for orientation C.

Incidentally, for diethylether adsorption onto Au(100) surface b was found to be 14.5 V^{-2} [15]. This value agrees well with that found for orientation A of adsorbed pyridine. This agreement is expected since the value of $(C_o - C_{\theta=1})$ should be similar for the two cases.

Finally, the differences between the pyridine adsorption at Au and at Hg surfaces can be stressed. At the gold electrode the flat adsorption of the pyridine molecules is observed at negative and vertical orientation at positive rational potentials. In contrast, on a mercury electrode the flat orientation is observed at positively and the vertical at the negatively charged surface [18]. This shows that the nature of the substrate is important in determining the characteristics of pyridine adsorption.

In this article we have employed the macroscopic model of the interface and we emphasized the role of the solute in the adsorption of organic molecules. In constrast, microscopic models developed by Bockris et al., [29, 30] aand recently by Guidelli et al., [31, 32] stress the role played by the solvent in determining the characteristics of the adsorption of organic molecules from aqueous solutions. In our next contribution, we shall compare the macroscopic and the microscopic models on the basis of extended spectroscopic experimental data, including the results obtained for

pyridine adsorption on various crystallographic orientations of gold.

ACKNOWLEDGEMENTS

This work was supported by grants from the Natural Sciences and Engineering Research Council of Canada and the Office of Naval Research (U.S.A.).

TABLE 1: Adsorption parameters for pyridine adsorbed on Au(100), polycrystalline Au and Hg electrodes

	Au(100)		Polycrystalline	
	Orientation A	Orientation C	Au[2]	Hg
$E_{max} - E_{pzc}$/V vs SCE	-0.09	0.26	-	--0.4V
σ_{max}/μC cm^{-2}	-4	+34	-	variable between -6 and -10
E_N/V	+0.02	-0.8	-0.3	+0.3
ΔG_A^{max}/kJmol^{-1}	-36	-	-38	-19
b/V^{2-}	14	25	-	-
Γ_{max} x 10^{10}mol cm^{-2}	assumed 3	6	-7	6.5
E_{pzc}/V vs SCE	+0.14	+0.14	+0.05	-0.5

Data for Hg electrode evaluated from results published in references [18, 20, 25]

REFERENCES

1. H. Baltruschat, E. Rach and J. Heitbaum, J. Electroanal. Chem., 194(1985) 109.
2. L. Stolberg, J. Richer, J. Lipkowski and D.E. Irish, J. Electroanal. Chem., 207(1986) 213.
3. a. A. Hamelin, G. Valette, C.R. Acad. Sc. Paris, Série C 267(1968) 211.

   b. A. Hamelin, J. Electroanal. Chem., 144(1983) 365.
4. A. Hamelin, in Modern Aspects of Electrochemistry, B.E. Conway, R.E. White and J. O'M Bockris, editors, Vol 16, 1(1985), Plenum Press, New York.
5. J. Clavilier, J. Electroanal. Chem., 107(1980) 211.
6. D. Dickertmann, J.W. Shultze and F.D. Koppitz, Electrochim. Acta, 21(1976) 967.
7. D.M. Kolb, G. Lehmpfuhl and M.S. Zei, J. Electroanal. Chem., 179(1984) 289.
8. a. D.M. Kolb and J. Schneider, Surface Sci. 162(1985) 764.

   b. D.M. Kolb and J. Schneider, Electrochim Acta 31(1986) 929.
9. A. Hamelin, Electrochim Acta 31(1986) 937.
10. a. J. Richer, L. Stolberg and J. Lipkowski, Langmuir, 2(1986) 630.

    b. J. Richer and J. Lipkowski, J. Electrochem. Soc., 133(1986) 121.
11. a. A. Hamelin and A. Le Lan, C.R. Acad. Sci. (Paris), 295, Serie 11(1982) 161.

    b. A. Hamelin, J. Electroanal. Chem. 142(1982) 299.
12. a. A. Hamelin and J. Lecoeur, Collect. Czech. Chem. Commun., 36(1971) 714.

    b. A. Hamelin and J. Lecoeur, Surf. Sci., 57(1976) 771.
13. J. Lecoeur, J. Andro, R. Parsons, Surf. Sci., 114(1982) 320.

14. R. Payne, J. Electroanal. Chem., 41(1973) 277.

15. B. Damaskin, A. Frumkin and A. Chizhov, J. Electroanal. Chem., 28(1970) 93.

16. J. Lipkowski, C.N. Van Huong, C. Hinnen, R. Parsons and J. Chevalet J. Electroanal. Chem., 143(1983) 375.

17. R. Parsons, Proc. R. Soc. Ser. A., 261(1961) 79.

18. B.E. Conway, R.G. Barradas, P.G. Hamilton and J.M. Parry, J. Electroanal. Chem., 10(1965) 485.

19. E. Dutkiewicz, J.D. Garnish and R. Parsons, J. Electroanal. Chem., 16(1968) 505.

20. B.E. Conway, J.G. Mathieson and H.P. Dhar, J. Phys. Chem., 78(1974) 1226.

21. R. Parsons, J. Electroanal. Chem., 7(1964) 136.

22 a. D.M. Mohilner, H. Nakadomari and P. Mohilner, J. Phys. Chem., 81(1977) 244.

b. J. Jastrzebska, M. Jurkiewicz-Herbich and S. Trasatti, J. Electroanal. Chem., 216(1987) 21.

23. K.J. Vetter and J.W. Schultze, Ber. Bunsenges. Phys. Chem., 76(1972) 920.

24. J.E. Demuth, K. Christmann and P.N. Sanda, Chem. Phys. Letters, 76(1980) 201.

25. R.G. Barradas and B.E. Conway, Electrochim. Acta, 5(1961) 349.

26. R.D. Armstrong, J. Electroanal. Chem., 20(1969) 168.

27. S. Trasatti, J. Electroanal. Chem., 53(1974) 335.

28. B.B. Damaskin and A.N. Frumkin, J. Electroanal. Chem., 34(1972) 191.

29. J. O'M. Bockris, M.A.V. Devanathan and K. Muller, Proc. R. Soc., London, Ser A, 274(1963) 55.

30. J. O'M. Bockris, E. Gileadi and K. Muller, Electrochim. Acta, 12(1967) 1301.

31. R. Guidelli, J. Electroanal. Chem., 197(1986) 77.

32. R. Guidelli, M.L. Foresti, J. Electroanal. Chem., 197(1986) 103.

List of Figures

Figure 1: Cyclic voltammograms recorded for (a) 0.1 M $KClO_4$ and (b) 0.1 M $KClO_4$ + 5 x 10^{-4} M pyridine. Sweep rate = 20 mVs^{-1}.

Figure 2: Differential capacity curves for (a) (●) 10^{-2} M $KClO_4$; (○) 0.1 M $KClO_4$ and (b) (●) 0.1 M $KClO_4$ + 1 x 10^{-4} M pyridine (■) 0.1 M $KClO_4$ + 6.2 x 10^{-3} M pyridine. Note for the sake of clarity not all experimental points are shown in the figure. Sweep rate = 5 mVs^{-1} and the ac modulation frequency = 25 Hz.

Figure 3: (a) Current-time transients recorded for a solution which contains 0.1 M $KClO_4$ + 6.2 x 10^{-3} M pyridine over the potential range -0.75 to +0.6 V. (b) Charge-time transients obtained by integration of the current-time transients shown in Fig 3a.

Figure 4: Charge density-potential curves which have been obtained for the following pyridine concentrations: (a) 6.2 x 10^{-3} M; (b) 2 x 10^{-3} M; (c) 10^{-3} M; (d) 3 x 10^{-4} M; (e) 10^{-4} M; (f) 3 x 10^{-5} M; (g) 10^{-5} M; (h) 0. Note that the data for the 10^{-2} M pyridine solution included later, on other plots, are not shown in this figure.

Figure 5: Film and surface pressure curves obtained at (A) constant potential and (B) constant charge for the following pyridine concentrations: (a) 10^{-2} M (b) 6.2 x 10^{-3} M (c) 2 x 10^{-3} M; (d) 10^{-3} M; (e) 3 x 10^{-4} M; (f) 10^{-4} M; (g) 3 x 10^{-5} M; (h) 10^{-5} M.

Figure 6: Surface concentration-potential curves obtained for the following pyridine concentrations: (a) 10^{-2} M; (b) 6.2 x 10^{-3} M; (c) 2 x 10^{-3} M; (d) 10^{-3} M; (e) 3 x 10^{-4} M; (f) 10^{-4} M; (g) 3 x 10^{-5} M; (h) 10^{-5}. Note: the

dashed lines represent a region of uncertainty in the value of the surface concentration.

Figure 7: Adsorption isotherms which have been obtained at the following electrode potentials. (a) -0.45 V; (b) -0.40 V; (c) -0.35 V; (d) -0.30 V; (e) -0.25 V; (f) -0.20 V; (g) -0.15 V; (h) -0.10 V; (i) -0.05 V; (j) 0V; (k) +0.05V. (l) +0.10 V.

Note: the dashed lines represent a region of uncertainty in the value of the surface concentration.

Figure 8: Plots of rational potential drop versus surface concentration for the various charge densities in $\mu C\ cm^{-2}$ indicated.

Figure 9: Plot of $-\Delta\bar{G}$ versus E as obtained from the Henry's law isotherm.

Figure 10: Plots of σ_M versus Γ at constant E for the determination of the electrosorption valency. The following electrode potentials are shown: (●) -0.475 V; (▲) -0.425 V; (□) -0.375 V; (X) -0.325 V; (*) -0.275 V; (o) -.225 V; (Δ) -0.175 V; (■) -0.125 V; (x) -0.075 V; (⊡) 0 V; (⊙) +0.05 V.

Figure 11: Comparison of the electrosorption valencies determined from ( ) differentiation of the σ_M versus Γ curves of Figure 10 and (o) by differentiation of the $\Delta\bar{G}$ - E curve of Figure 9.

Figure 12: (a) Comparison of the differential capacity curves obtained for gold(100) in (dotted line) 0.1 M NaF + 10^{-3} M pyridine and (solid line) 0.1 M $KClO_4$ + 10^{-3} M pyridine (b) Comparison of the charge density-potential curves which have been obtained for (solid line) 0.1 M $KClO_4$ + 10^{-3} M pyridine and (---X---) 0.1 M NaF + 10^{-3} M pyridine solutions.

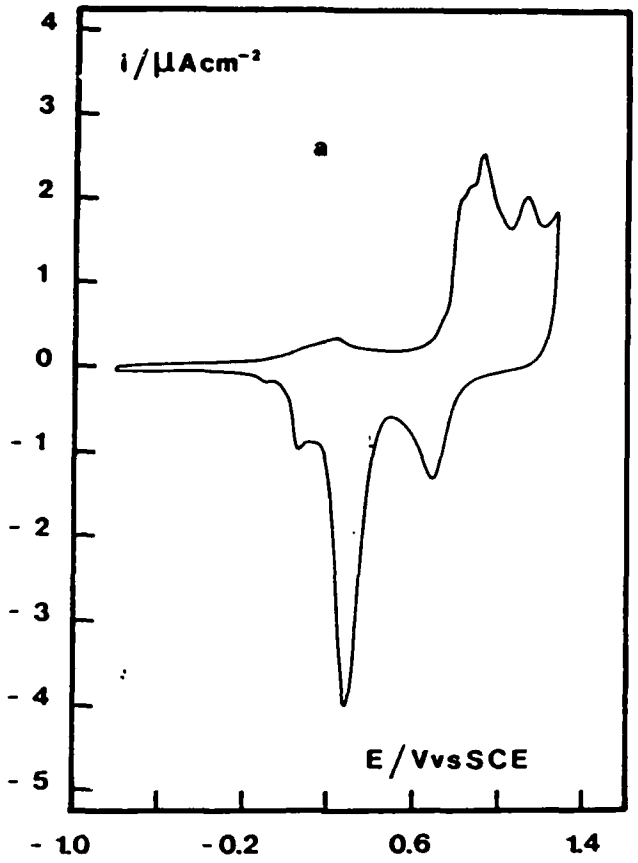
i/μAcm⁻²
a
4
3
2
1
0
- 1
- 2
- 3
- 4
- 5
E/VvsSCE
- 1.0
- 0.2
0.6
1.4

Fig 1a

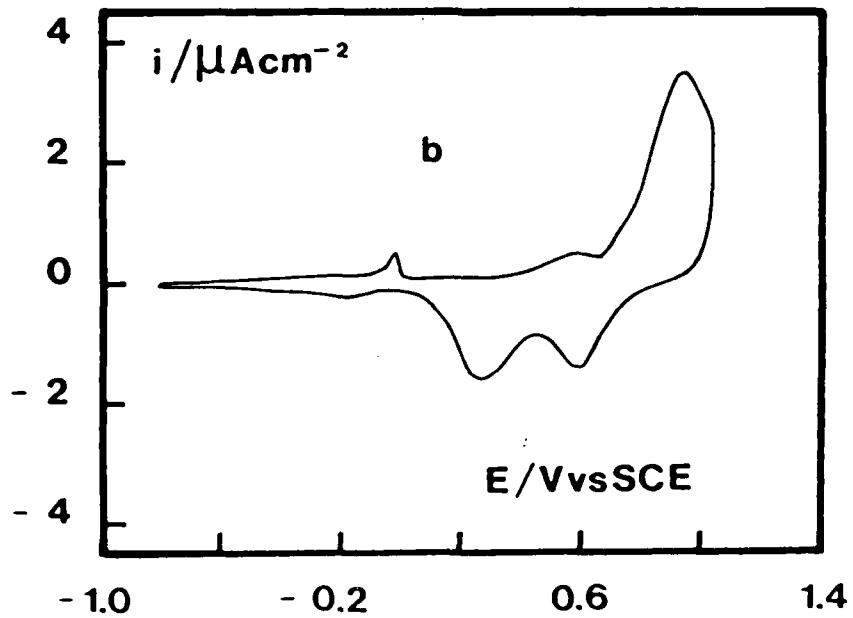
i/μAcm⁻²
b
4
2
0
- 2
- 4
E/VvsSCE
- 1.0
- 0.2
0.6
1.4

Fig 1b

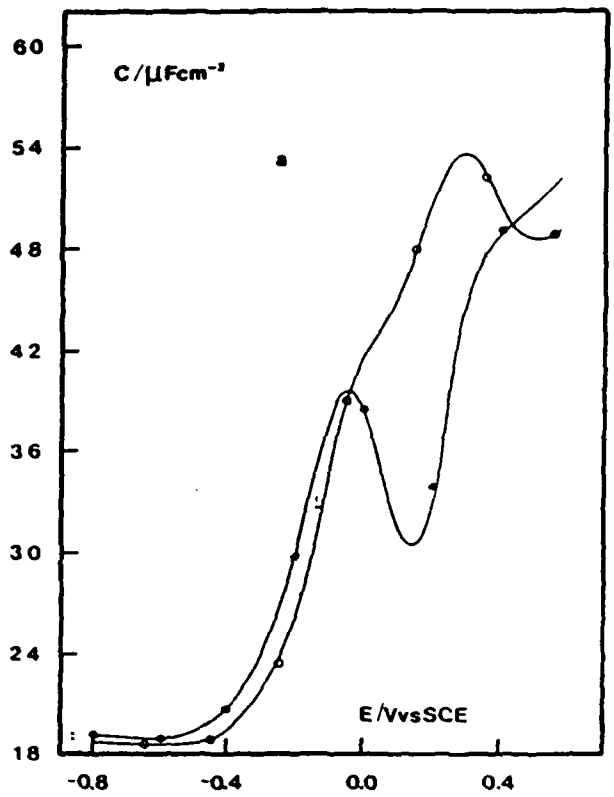
C/μFcm⁻²
a
60
54
48
42
36
30
24
18
E/VvsSCE
-0.8
-0.4
0.0
0.4

Fig 2a

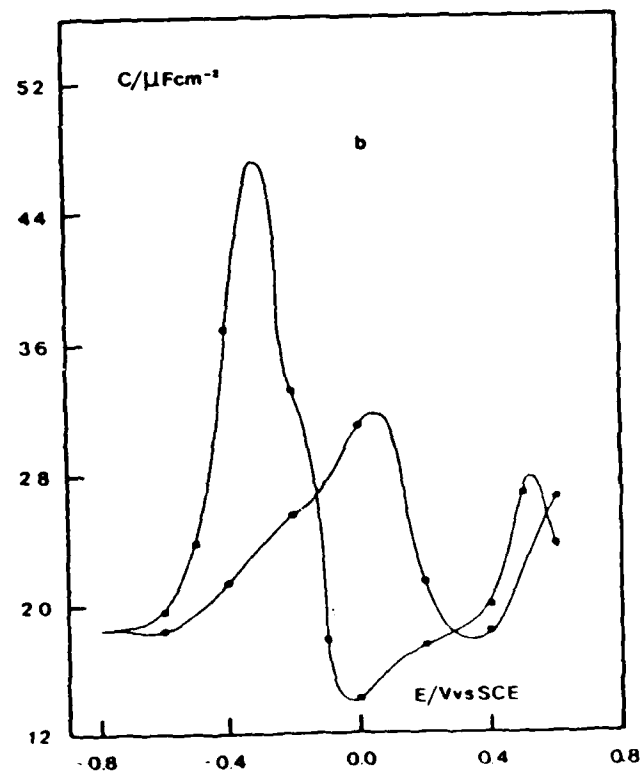
C/μFcm⁻²
b
52
44
36
28
20
12
E/VvsSCE
-0.8
-0.4
0.0
0.4
0.8

Fig 2b

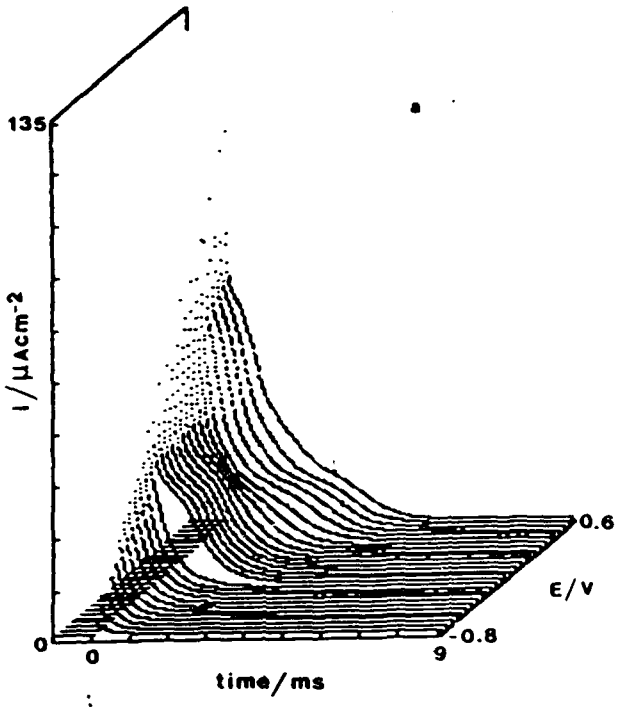
a
135
0
I/μAcm⁻²
0
9
time/ms
0.6
E/V
-0.8

Fig 3a

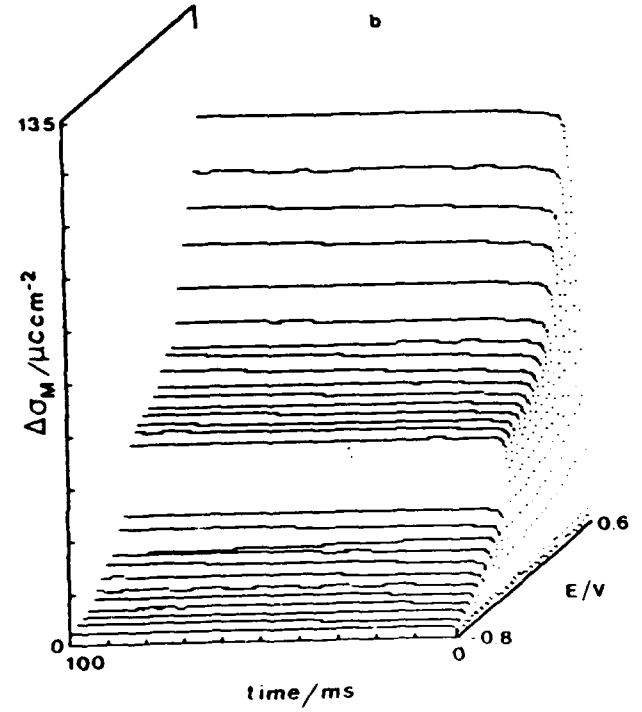
b
135
0
Δσ_M/μCcm⁻²
100
0
time/ms
0.6
E/V
-0.8

Fig 3b

Fig 4

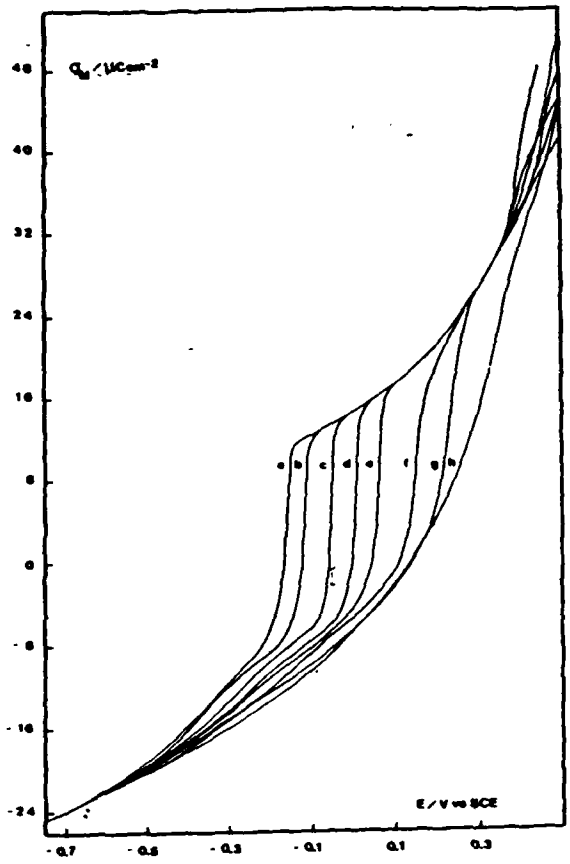

Fig 5

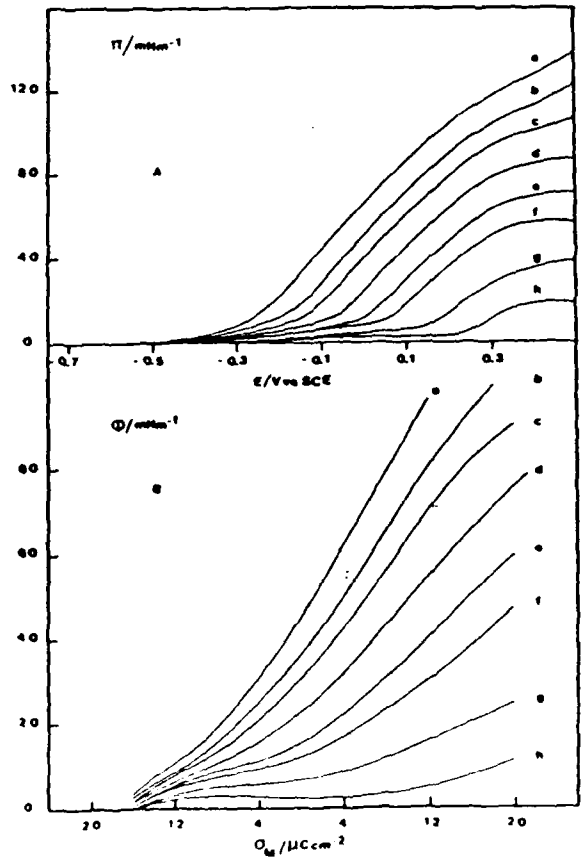

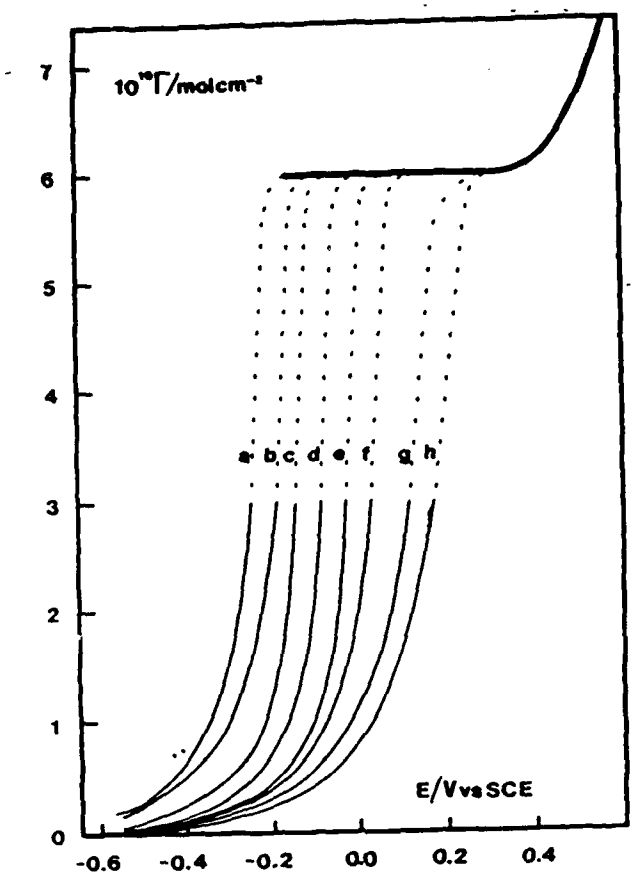
$10^{10}\Gamma$/molcm^{-2}
7
6
5
4
3
2
1
0
a b c d e f g h
E/V vs SCE
-0.6
-0.4
-0.2
0.0
0.2
0.4

Fig 6

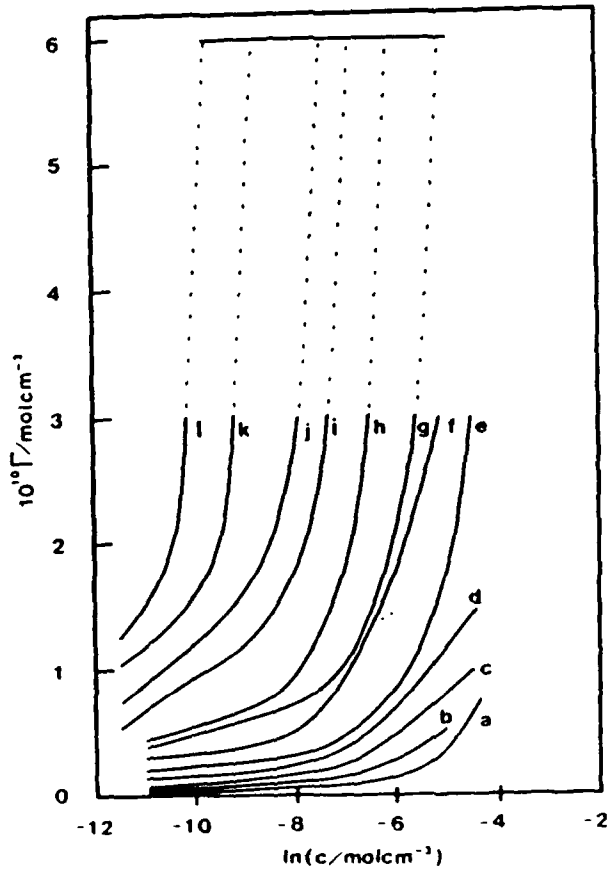
$10^{9}\Gamma$/molcm^{-2}
6
5
4
3
2
1
0
l k j i h g f e
d
c
b
a
-12
-10
-8
-6
-4
-2
ln(c/molcm^{-3})

Fig 7

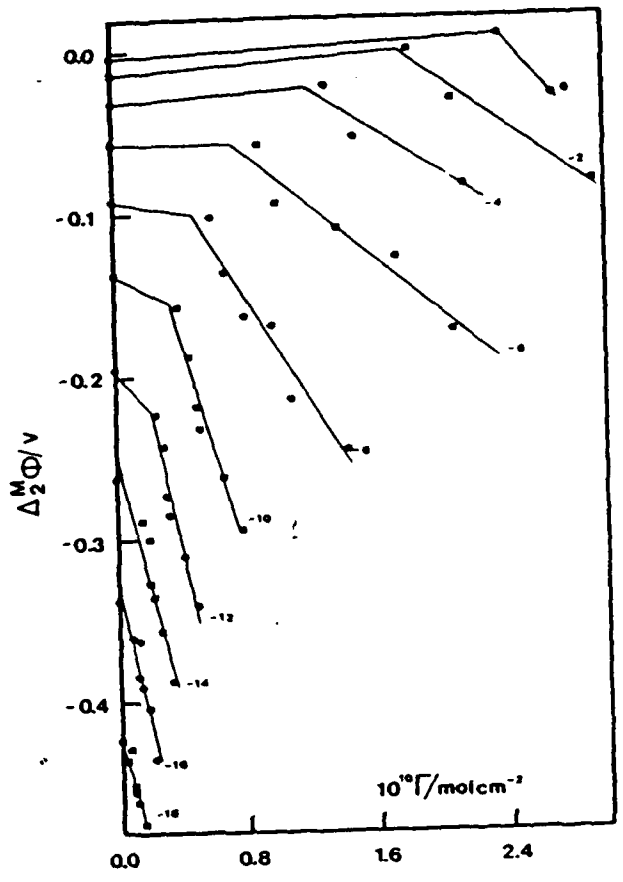
0.0
-0.1
-0.2
-0.3
-0.4
$\Delta_2^M\Phi$/v
-2
-4
-6
-8
-10
-12
-14
-16
-18
$10^{10}\Gamma$/molcm^{-2}
0.0
0.8
1.6
2.4

Fig 8

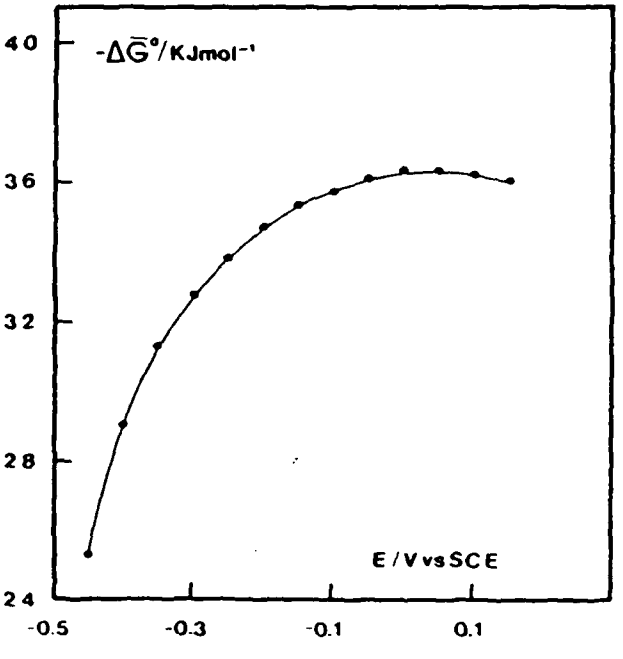
40
36
32
28
24
$-\Delta\bar{G}^{\circ}$/KJmol^{-1}
E/VvsSCE
-0.5
-0.3
-0.1
0.1

Fig 9

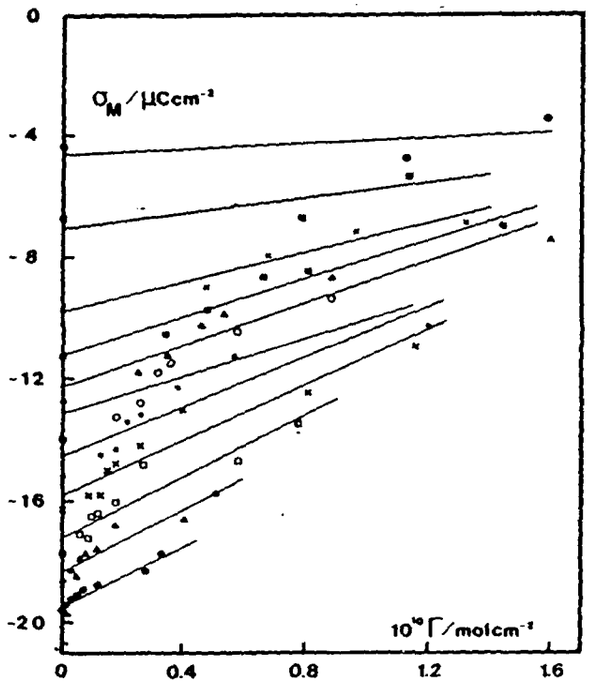
0
-4
-8
-12
-16
-20
σ_M / μCcm⁻²
$10^{10}\Gamma$ / molcm⁻²
0
0.4
0.8
1.2
1.6

Fig 10

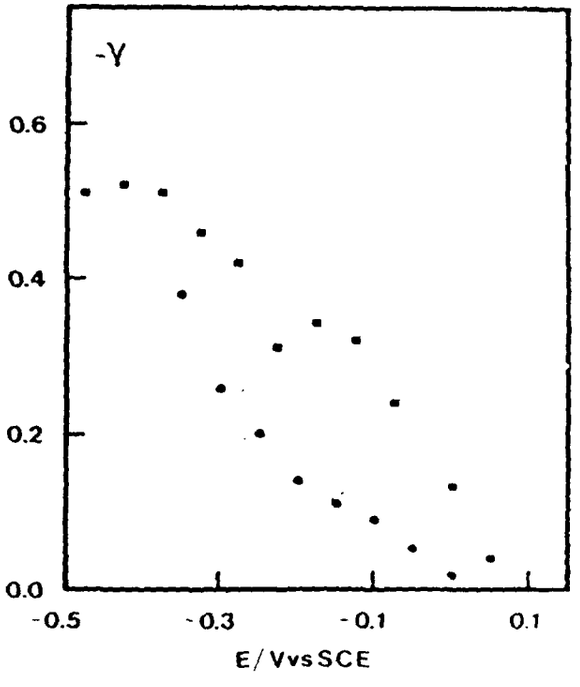
-Y
0.6
0.4
0.2
0.0
-0.5
-0.3
-0.1
0.1
E / V vs SCE

Fig 11

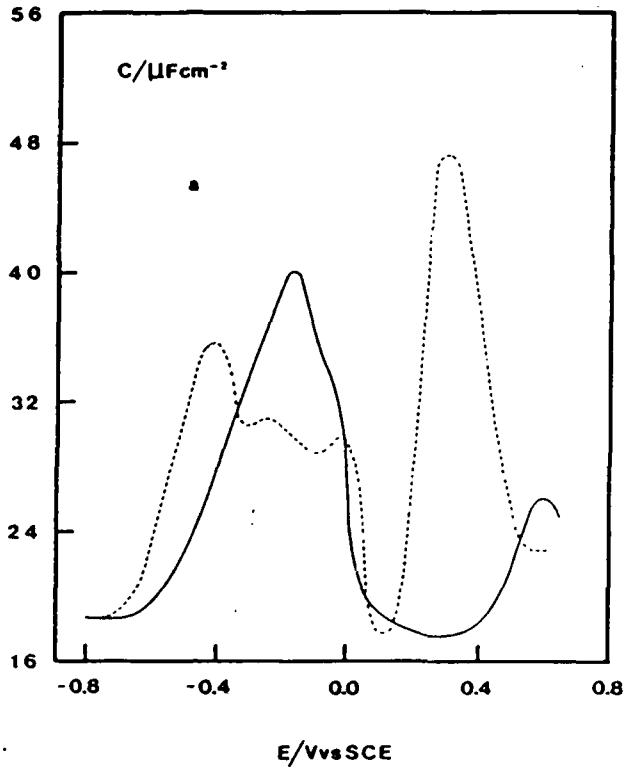

Fig 12a

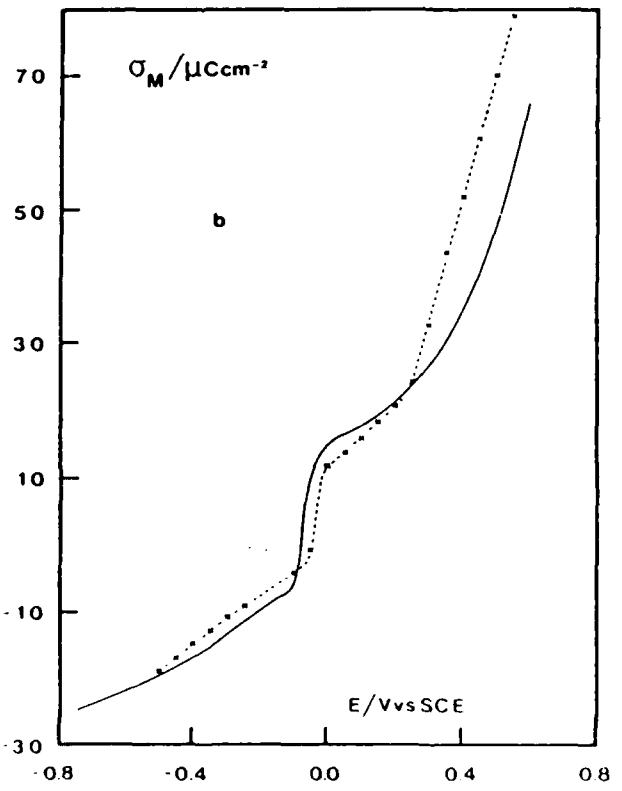

Fig 12b

DL/1113/87/2

TECHNICAL REPORT DISTRIBUTION LIST, GEN

	No. Copies
Office of Naval Research Attn: Code 1113 800 N. Quincy Street Arlington, Virginia 22217-5000	2
Dr. Bernard Douda Naval Weapons Support Center Code 50C Crane, Indiana 47522-5050	1
Naval Civil Engineering Laboratory Attn: Dr. R. W. Drisko, Code L52 Port Hueneme, California 93401	1
Defense Technical Information Center Building 5, Cameron Station Alexandria, Virginia 22314	12 high quality
DTNSRDC Attn: Dr. H. Singerman Applied Chemistry Division Annapolis, Maryland 21401	1
Dr. William Tolles Superintendent Chemistry Division, Code 6100 Naval Research Laboratory Washington, D.C. 20375-5000	1
Dr. David Young Code 334 NORDA NSTL, Mississippi 39529	1
Naval Weapons Center Attn: Dr. Ron Atkins Chemistry Division China Lake, California 93555	1
Scientific Advisor Commandant of the Marine Corps Code RD-1 Washington, D.C. 20380	1
U.S. Army Research Office Attn: CRD-AA-IP P.O. Box 12211 Research Triangle Park, NC 27709	1
Mr. John Boyle Materials Branch Naval Ship Engineering Center Philadelphia, Pennsylvania 19112	1
Naval Ocean Systems Center Attn: Dr. S. Yamamoto Marine Sciences Division San Diego, California 91232	1

END

FEB.

1988

DTIC